catalysts

MDPI

Article

Dynamic EPR Studies of the Formation of Catalytically Active Centres in Multicomponent Hydrogenation Systems

Yuliya Yu. Titova

A.E. Favorsky Irkutsk Institute of Chemistry, Siberian Branch of Russian Academy of Sciences, 1 Favorsky Street, 664033 Irkutsk, Russia; ytitova60@rambler.ru or titova@irioch.irk.ru; Tel.: +7-3952-426911

Abstract: The formation of catalytically active nano-sized cobalt-containing structures in multicomponent hydrogenation systems based on $Co(acac)_2$ complex and various cocatalysts, namely, $AlEt_3$, $AlEt_2(OEt)$, Li-*n*-Bu, and $(PhCH_2)MgCl$, has been studied for the first time in detail using dynamic EPR spectroscopy. It is shown that after mixing the initial components, paramagnetic structures are formed, which include a fragment containing Co(0) with the electronic configuration $3d^9$, as well as a fragment bearing an aluminium, lithium, or magnesium atom, depending on the nature of the used cocatalyst. Such bimetallic paramagnetic sites are stabilized by acetylacetonate ligands. In addition, the paramagnetic complex contains the arene molecule(s), and the cobalt atom is bonded with the atom of the corresponding non-transition through the alkyl group of the co-catalyst, in particular through the carbon atom in the α-position with respect to the atom of the non-transition element. Due to the high reactivity of the described intermediates, they, under the conditions of hydrogenation catalysis, are transformed into nano-sized cobalt-containing structures that act as carriers of the catalytically active sites. Furthermore, because of the high reactivity and paramagnetism, such intermediates can be detected only by the EPR technique. The paper describes the whole experimental way of interpreting the EPR signals corresponding to the intermediates, precursors of catalytically active structures. In addition, a possible mathematical model based on the obtained experimental EPR data is presented.

Keywords: EPR study; multicomponent catalytic systems; intermediate; paramagnetic structures; arene complex; cobalt complex; mathematical simulation

Citation: Titova, Y.Y. Dynamic EPR Studies of the Formation of Catalytically Active Centres in Multicomponent Hydrogenation Systems. *Catalysts* **2023**, *13*, 653. https://doi.org/10.3390/catal13040653

Academic Editors: Victorio Cadierno, Raffaella Mancuso and Kotohiro Nomura

Received: 18 October 2022
Revised: 13 March 2023
Accepted: 24 March 2023
Published: 27 March 2023

1. Introduction

Currently, electron paramagnetic resonance (EPR), or electron spin resonance (ESR) spectroscopy, is one of the most accurate methods [1] allowing the determination of the types of magnetic nuclei with which an unpaired electron interacts in various structures, ranging from organic [2–4], inorganic [5,6] and organometallic [6–8] radicals to coordination complexes [4,9,10] and biological macromolecules [11–13] containing a paramagnetic centre. The EPR signal intensity depends on the number of spins. Therefore, this method, like any other spectroscopic technique, can be employed analytically to determine the concentration of paramagnetic particles [14–17]. Such analytical applications commonly require a reference sample for the creation of a calibrated intensity scale. In some cases, EPR spectroscopy can be exploited for the evaluation of a chemical reaction rate or conformational change rate [18–20]. All the above enables consideration of the EPR approach as an almost indispensable tool for a detailed study of the formation and functioning of catalytically active species at the molecular level.

In the literature, there are reviews devoted to the application of EPR spectroscopy in enzymatic [21–23], homogeneous [22–24], heterogeneous and/or nanoscale [23,25–28] catalysis. Generally, these reviews summarize the employment of EPR in investigations of specific catalysts. In the present work, multicomponent catalytic hydrogenation systems were chosen as model ones. These systems are formed from at least two components,

each of which does not exhibit catalytic activity separately under the given conditions. Upon mixing the components, the structures, active in the catalytic processes, e.g., in hydrogenation and/or oligo-/polymerization of unsaturated hydrocarbons, are formed. Among the best known such systems are Ziegler-type catalysts [29–32] or Brookhart compositions [33–35]. This choice is non-random. First, these systems show catalytic activity in various industrially important chemical transformations, namely in hydrogenation, oligo- and polymerization, as well as isomerization of unsaturated compounds, the nature of the catalytically active centres being dependent, inter alia, on the type of reactions [29,30,32,35]. Second, variation in the structure and conditions of the formation and/or functioning of such systems allows one to obtain, in one reaction operation, the compounds that have paramagnetic properties of organic radicals and organometallic complexes, as well as ferromagnetic characteristics of nano-sized particles. Consequently, the reactivity of these systems can be compared under the same conditions. As a result, the data of EPR and kinetic studied, obtained from one experiment, enable reliable description of the processes occurring at the stages of catalyst formation and functioning. A major drawback of this approach is that the samples of the analysed systems should studied ex situ, taking samples in the course of the experiment. Given that most of the intermediates that are generated at the stage of catalytically active sites formation are highly reactive substances, the nature of which depends, among other things, on the method of sampling, some error may arise in the quality of the obtained results. Therefore, to improve the reliability of the results, it makes sense to perform, apart from careful experiments, a reasonable number of repetitions of each specific model test. It should be noted that today, catalytically active systems can already be analysed in situ [36–39]. One can hope that in the future, the wide application of these techniques will significantly expand the potential of research.

A large body of evidence on the formation and functioning of multicomponent systems for oligo- and polymerization of α-olefins was reported [36,40–44]. Noteworthily, the EPR spectroscopy played a crucial role in these studies. For example, the EPR technique was employed for the investigation of nickel- [45–49], chromium- [50], cobalt- [51,52], and iron- [53,54] containing multicomponent systems, etc. [55–61]. On the other hand, EPR spectroscopy is less often used for the study of multicomponent hydrogenation systems. Meanwhile, from a historical perspective, multicomponent catalytic systems were first applied just to the hydrogenation processes [62–64]. Further milestones in the development of hydrogenation catalysis using the multicomponent catalytic systems were summarized in detail in the review [29] and, therefore, they remained beyond the scope of the present. It should only be mentioned that almost all studies carried out over the past 20–30 years (i.e., the studies performed using high-precision analytical equipment) show that $M(0)_n$ particles are formed during the formation or functioning of the catalytic system. The size of these particles depends on many parameters, e.g., the nature of each component of the catalytic composition, the order and method of the component mixture, the character of the solvent, the substrate and time of its introduction into the reactor, hydrogenation temperature, hydrogen pressure, and the presence of impurities in the reaction system, namely, specially introduced ligands, air oxygen, water, etc. [29,65–70]. Interestingly, the components acting as cocatalysts (as a rule, these are aluminium, lithium or magnesium organic compounds, as well as complex metal hydrides) play the role of not only the reducing agents, but also stabilizers of the transition metal species formed, as well as inhibitors of catalytic activity [69,70]. Among the only true homogeneous multicomponent catalysts of hydrogenation are the systems based on $(Cp)_2TiCl_2$ + $nAlEt_3$ [71], in which titanium(III) hydrides $\{(Cp)_2Ti\text{-}H\}$ are assumed to be catalytically active complexes, as well as the compositions described by Müttertiz et al. [72–74], i.e., allylcobalt complexes η^3 -$C_3H_5CoL_3$, where L is a phosphine or phosphite ligand. In addition, it cannot be ruled out that in multicomponent hydrogenation systems, both homogeneous (for example, if the nanoparticles are soluble in the solvent(s) used or the formed active in catalysis complexes work according to FLP mechanism [75,76]) and microheterogeneous/nanosized centres will possess activity [70]. Moreover, in the case of the microheterogeneous/nanosized

particles, both surface transition metal atoms M(0) and supported metallocomplexes, which represent in essence the transition state between a mixture of the initial components and $M(0)_n$ particles, can exert catalytic activity.

In this vein, of special interest are two catalytic systems formed in situ from $M(acac)_2$ and $AlEt_3$, where M = Ni or Co. It is established that, when the compounds with "reachable" degree of purity (water content does not exceed 2 mmol/L) are employed as the initial components (solvents, $Ni(acac)_2$, $Co(acac)_2$, substrate(s) and gases), homogeneous solutions, stable without air or moisture, are formed. Such compositions are found to be catalytically inactive at all [68–70]. Here, $Ni(acac)_2$ or $Co(acac)_2$ are reduced to the state of Ni(0) and Co(0), respectively. The addition of water or other proton-donor solvents heterogenises these compositions and leads to an appearance of an increase in the catalytic activity. The TOF and TON of both systems in hydrogenation of, for example, the model styrene compound, are approximately the same. In both cases, the carriers of catalytic activity are proven to be nano-sized particles, consisting of a metal core (0.7–5 nm) stabilized by a ligand shell. The ligand shell contains acetylacetonate compounds of aluminium and $AlEt_3$ that are bound to the surface metal atoms by an acid-base interaction. However, the mechanisms of formation of these particles are completely different [68–70].

The combined study using EPR technique, kinetic research, UV, IR, TEM HR, electron diffraction and energy dispersive X-ray analysis has shown that the interaction of $Ni(acac)_2$ with $AlEt_3$ under mild conditions (T = 30 °C, P_{H2} = 2 atm) involves the reduction of nickel to zerovalent state, while the reaction solution remains homogeneous (ferromagnetic resonance signal in the EPR spectrum and high-contrast regions on the TEM HR micrographs are absent). The addition of water or another proton-donor compound to the reaction system leads to the appearance and growth of a ferromagnetic resonance signal, the intensity of which increases as the catalytic activity enhances [68–70]. The analysis of particle size distribution histograms indicates that the growth of the particle size may be due to the diffuse aggregation.

It is noteworthy that the study of the system formed from $Co(acac)_2$ and $AlEt_3$ by UV, IR, TEM HR methods as well as kinetic experiments gave almost similar results. However, the data obtained using the EPR are fundamentally different. Immediately after mixing the initial components of the system based on $Co(acac)_2$ and Red (where Red = $AlEt_3$), characteristic signals were recorded in the EPR spectra (at T = 77 K). The signals were previously attributed to the cobalt complexes in formally zero oxidation state [66,69,71,77].

Despite the fact that these structures have been described in a number of works [67,70,72,78], the issue concerning their nature and a role in hydrogenation catalysis remains open. The reason is that the EPR technique (at T = 77 K) is almost the only method suitable for detection of such structures. Therefore, to obtain additional information, in this work, we have employed a combined approach comprising kinetic experiments and EPR studies, as well as the mathematical simulation technique. Previously, the efficiency of such approach was demonstrated for the multicomponent nickel-containing systems of ethylene oligo- and polymerization [78]. However, this approach will be used to study multicomponent hydrogenation systems for the first time. Accordingly, the application of this methodology will originally permit to present in dynamics the entire process of the formation of cobalt-containing sites catalytically active in hydrogenation through the generation of intermediates. The findings disclosed in the paper, on the one hand, will gain insight into the still poorly studied formation of the multicomponent hydrogenation systems, and on the other hand, will contribute to the development of methodologies for dynamic EPR spectroscopy. The first part of the work describes the obtained experimental facts, while the second one deals with the results of the mathematical simulation and provides the discussion of the experimental data.

2. Results

First of all, it should be noted that the characteristic EPR signals for systems based on $Co(acac)_2$ and Red (where Red = $AlEt_3$, $AlEt_2(OEt)$, Li-*n*-Bu, $(PhCH_2)MgCl$) are recorded

at T = 77 K. A detail study of each specific system has shown that the paramagnetic complex contains arene molecule(s), which may be used either as a solvent or be specially added to the system. Thus, the corresponding characteristic signal is detected during the formation of the $Co(acac)_2$—$AlEt_3$ system in a medium of saturated hydrocarbon (heptane) after the addition of arene already at a molar ratio of arene/Co = 1–2. It is found that the parameters of the EPR spectra depend on the number and position of alkyl substituents in alkylbenzenes. Figure 1 depicts such spectra obtained in the presence of toluene, p-xylene (1,4-dimethylbenzene), mesitylene (1,3,5-trimethylbenzene), and durene (1,2,4,5-tetramethylbenzene).

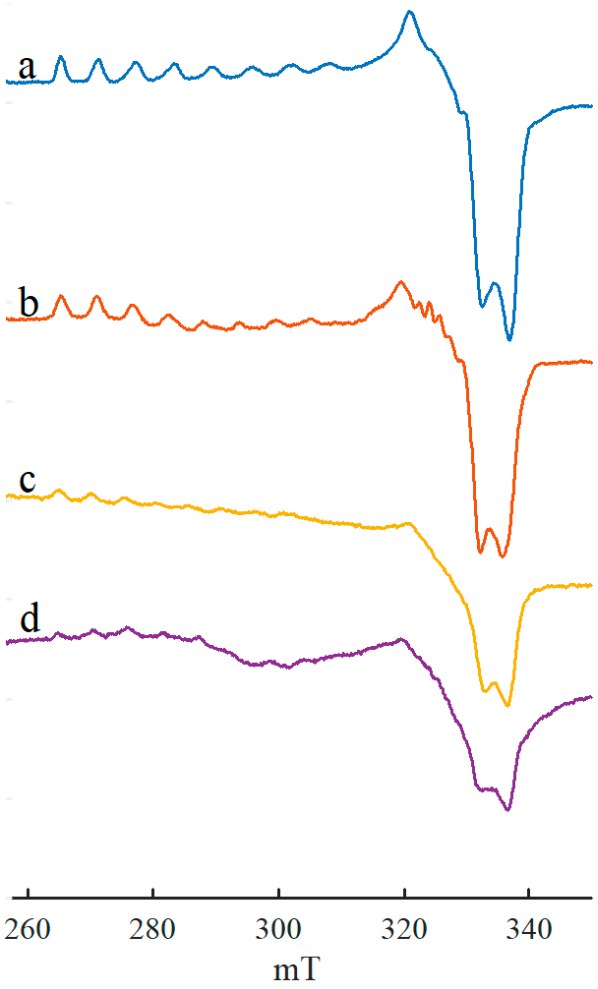

Figure 1. EPR spectra of the $Co(acac)_2$–$AlEt_3$ catalytic system formed in an argon atmosphere, other conditions being equal, in the presence of (a) toluene, (b) mesitelene, (c) p-xylene, (d) durene. Spectrum (a) was taken from [69,77].

The variation in the arene/Co ratio during the formation of $Co(acac)_2$—$AlEt_3$ systems in a heptane medium suggests that one or two arene molecules are coordinated to cobalt. This fact is confirmed by the results of other experimental and computational studies [79–83].

The dependence of intensity changes of the signals, recorded in the presence of toluene and mesitylene, on time is shown in Figures 2 and 3, respectively. It is found that changes in the signal intensities of systems formed in argon occur through a maximum. The stability of the considered paramagnetic signals depends on the nature of the arene. The signal of the $Co(acac)_2$–$AlEt_3$ system obtained in mesitylene is the most stable (see Figure 3). Quantitative analysis reveals that the maximum intensity of the paramagnetic signal corresponds to ~77% from the signal intensity of the initial $Co(acac)_2$.

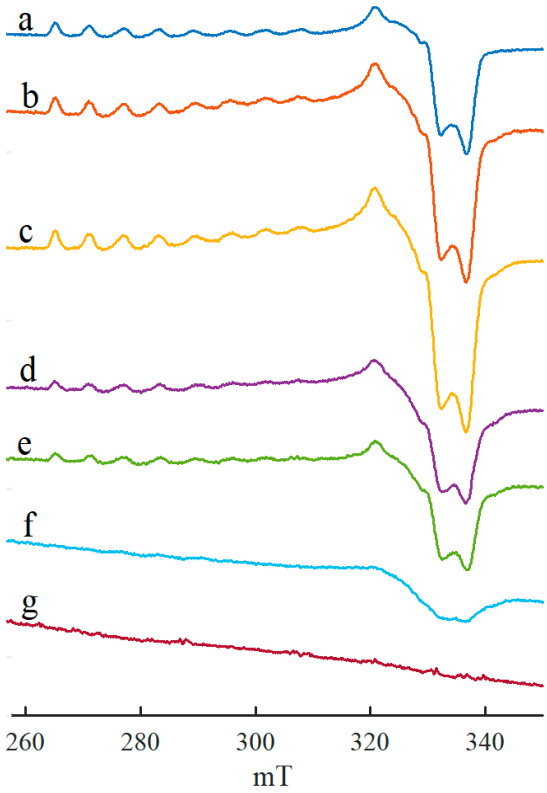

Figure 2. Time dependence of EPR spectra of the catalytic system formed on the basis of $Co(acac)_2$–$AlEt_3$ in toluene in an argon atmosphere under otherwise equal time conditions: (a) 0.1 min, (b) 0.5 min, (c) 1 min, (d) 5 min, (e) 10 min, (f) 15–45 min, (g) 60–90 min (Some spectra (Figure 2f,g, and et seq.), apart from the paramagnetic signals, contain a broadened ferromagnetic resonance signal. These signals are due to the transformation of paramagnetic intermediates into nano-sized cobalt-containing structures. The rate of the intermediate transformation into a nanostructure is determined, other things being equal, by the nature of the cocatalyst.). Spectrum (a) was taken from [77].

All spectra shown in Figures 1–3 and almost all other spectra discussed below, apart from the main signal, contain a ferromagnetic resonance signal, though very weak and very wide, since the right and left shoulders of each spectrum are at different heights. This signal is due to the rapid transformation of cobalt-containing complexes to cobalt-containing Co(Ar)(L) particles (where Ar is arene, L is $AlEt_3$ or $AlEt_2(acac)$). It was reported [69,70,77] that the formation of the cobalt-containing nanoparticles and their average size depend on the amount of water or other proton-donor compounds, which are present or specially introduced into the systems under study. Therefore, it can be assumed that the low-intensity, broadened ferromagnetic resonance signal is caused by trace amounts of water contained in the initial components and gases, as well as on the walls of reaction vessels and EPR ampoules. More reasonable assumptions cannot yet be made.

Although the complexes of Group 9 metals usually have weaker metal-arene bonds compared to the related compounds of Groups 6–8 [83,84], the generation of structures containing a Co-arene bond under the conditions of a multicomponent system formation is possible. Apparently, the formation of such bonds is a key factor in the production of paramagnetic cobalt-containing structures.

The parameters and/or intensity of the recorded signals, as well as the intensity of the ferromagnetic resonance signal, all other things being equal, also depend on the nature of the cocatalyst [69,77] (see Figure 4).

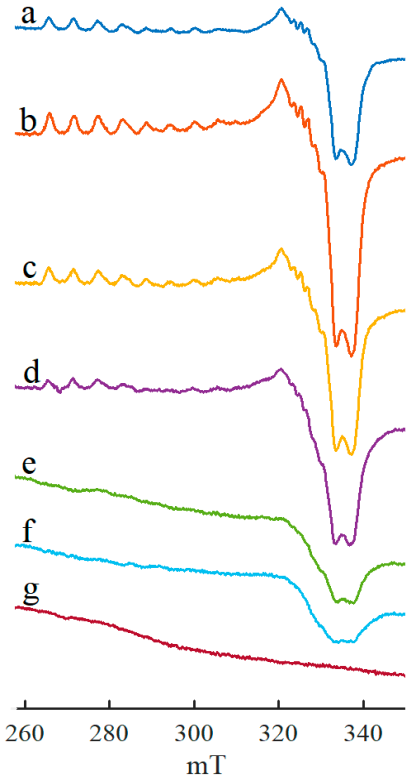

Figure 3. Time dependence of EPR spectra of the catalytic system formed on the basis of $Co(acac)_2$–$AlEt_3$ in mesitylene in an argon atmosphere under otherwise equal time conditions: (a) 0.1–1 min, (b) 5–15 min, (c) 15–25 min, (d) 25–45 min, (e) 45–80 min, (f) 80–160 min, (g) 200 min. Spectrum (a) was taken from [69].

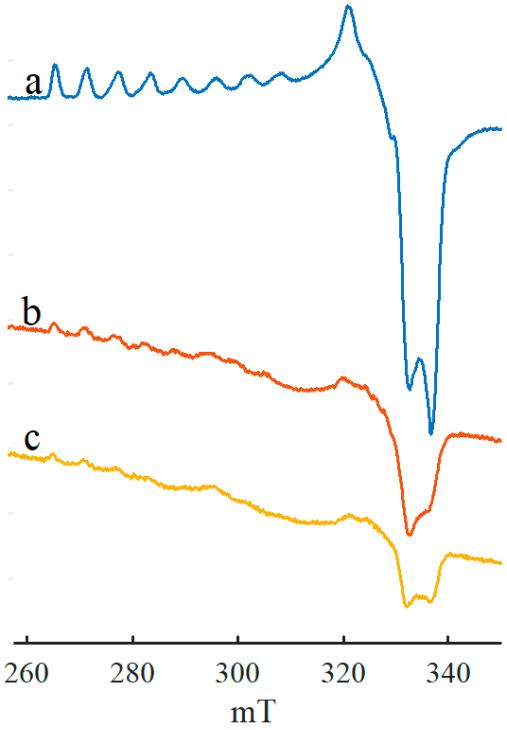

Figure 4. EPR spectra of the $Co(acac)_2$–Red catalytic system formed in an argon atmosphere, other conditions being equal, where (a) Red = $AlEt_3$, (b) Red = Li-*n*-Bu and (c) $(PhCH_2)MgCl$. Spectrum (a) was taken from [77].

For example, among the cocatalysts studied in this work, the most reproducible and well-resolved spectra were detected for the systems with triethylaluminum, while low-intensity signals were recorded for the systems based on magnesium and organolithium compounds at any ratio of the initial components. Moreover, for the systems formed in the presence of organolithium compounds, the intensity of EPR signals was higher than that of for the systems based on organomagnesium components. In addition, the maximum intensity of paramagnetic signals also depends on the nature of the cocatalyst. For instance, for the systems formed in the presence of $AlEt_3$, paramagnetic signals were observed at Al/Co $\geq$ 2; in the presence of Li-*n*-Bu—at Li/Co > 5–10; in the presence of $(PhCH_2)MgCl$—at Mg/Co > 10, in the presence of $AlEt_2(OEt)$—at Al/Co = 10.

Parameters of the cobalt-containing fragments of the EPR spectra, within the limits of measurement errors, do not depend on the nature of the non-transition element (see Figure 4). On the other hand, the signals of paramagnetic structures described above were not detected in the EPR spectrum for systems based on $Co(acac)_2$—Red, where Red = $LiAlH_4$ or $LiAlH(tert\text{-}OBu)_3$. In other words, the above paramagnetic centres can only be formed if the cocatalyst contains a M–carbon bond (where M = Al, Li, Mg), i.e., when cobalt is bonded with a non-transitional element through the alkyl group of the co-catalyst, in particular, through the α-carbon atom. Such compounds were previously documented by Wilke et al. [85].

It was found that paramagnetic signals were not detected, when compounds with monodentate anionic ligands, such as halides or alkoxides, were used as the initial cobalt complex. For comparison, the system based on a complex of cobalt dimethylglyoxymate was also studied. In this case, the attempts to record the spectra of paramagnetic structures also failed. This means that chelating oxygen-containing ligands in the initial cobalt complex play an important role in the formation of paramagnetic cobalt-containing structures.

It was shown that when $Co(acac)_2$ was replaced by crystalline hydrates, $Co(acac)_2 \cdot 0.5H_2O$ or $Co(acac)_2 \cdot 3.0H_2O$, in the $AlEt_3$-based system, the intensity of EPR signal decreased and the spectrum was distorted (Figure 5) compared to the intensity of the signal recorded for the of $Co(acac)_2$-based systems (see Figure 5). When $AlEt_2(OEt)$ was used as a cocatalyst, a strongly distorted signal was observed in the EPR spectrum (see Figure 5d), apparently due to changes in the geometry of the structure caused by the replacement of the Et-fragment for the OEt-group. Figure 5e shows also the spectrum of the $Co(acac)_2$–$AlEt_3$–3*n*-BuOH system. To record this spectrum, the $Co(acac)_2$–$AlEt_3$ system was obtained as a preliminary step; its spectrum is shown in Figure 5a, then the calculated amount of alcohol was added to this system. The EPR sample was taken immediately after the addition of *n*-BuOH, other things being equal. In other words, the introduction of butanol led to complete disappearance of the signal from the paramagnetic structure.

When the components of the $Co(acac)_2$-$AlEt_3$ system interact in a hydrogen atmosphere, a more than twofold decrease in the initial intensity of the paramagnetic signal in the EPR spectrum and its complete disappearance after 4 min are observed (see Figure 6). It should be noted that under the same reaction conditions, but in an argon atmosphere, the EPR signals of the paramagnetic structures formed in toluene were detected for at least 45 min (see Figures 1–3). This can be explained by the fact that the intermediate cobalt alkyl complexes are highly reactive compounds. The reactions of LCoEt hydrogenolysis (L = arene, $AlEt_3$, and $AlEt_2(acac)$) or oxidative addition of a hydrogen molecule to Co(0) lead to a rapid loss of paramagnetism under the conditions of hydrogenation catalysis.

Previously, it was shown [66] that the addition of an olefin, for example, hexene-1, to the $Co(acac)_2$–$AlEt_3$ system transformed one signal in the EPR spectrum into another one. It was assumed that this phenomenon is due to the substitution of acetylacetonate ligand in the first coordination sphere of the cobalt atom by the olefin molecule. In the present work, we failed to reproduce these results for the formation of the $Co(acac)_2$–$AlEt_3$ system either in argon or in hydrogen. It was found that when 1-hexene was added to the $Co(acac)_2$–$AlEt_3$ system formed in argon, the intensity of the signal from paramagnetic centres dropped sharply, while the signal shape was distorted (see Figure 7a–d). The signal

of the paramagnetic complex was almost unobserved (Figure 7e) if styrene was used as a substrate. When the $Co(acac)_2$–$AlEt_3$ system was formed in a hydrogen atmosphere, the addition of 1-hexene sharply reduced intensity of the paramagnetic signal, and in the first minute after the hydrogenation started, the signal disappeared completely.

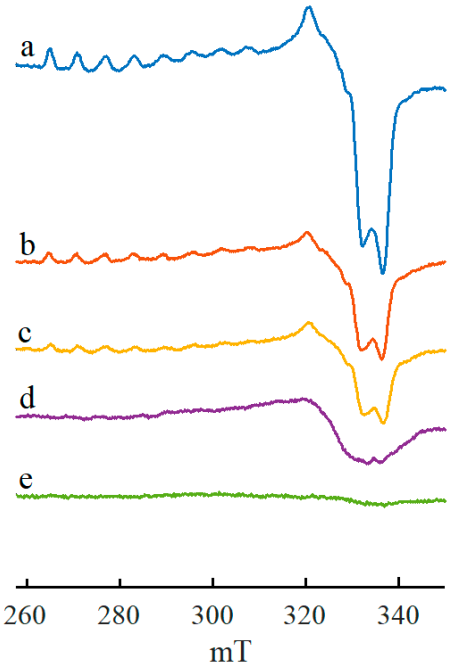

Figure 5. EPR spectra of the catalytic system formed on the basis of $AlEt_3$ in an argon atmosphere, (a) $Co(acac)_2$, (b) $Co(acac)_2 \cdot 0.5H_2O$, (c) $Co(acac)_2 \cdot 3.0H_2O$, (d) $Co(acac)_2$–$AlEt_2(OEt)$ and (e) $Co(acac)_2$–$AlEt_3$–3*n*-BuOH. Spectra were obtained under identical conditions. Spectra (a,b) were taken from [69,77].

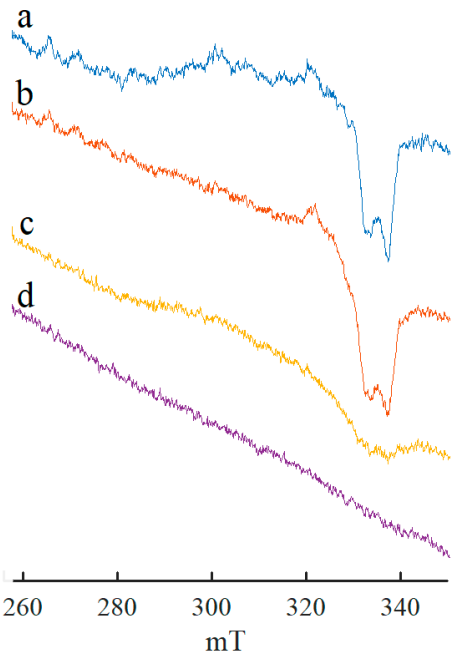

Figure 6. EPR spectra of the $Co(acac)_2$–$AlEt_3$ catalytic system formed in toluene in a hydrogen atmosphere: (a) 0.1–1 min, (b) 1–2 min, (c) 2–3 min, and (d) 4 min. Spectra were obtained under identical conditions.

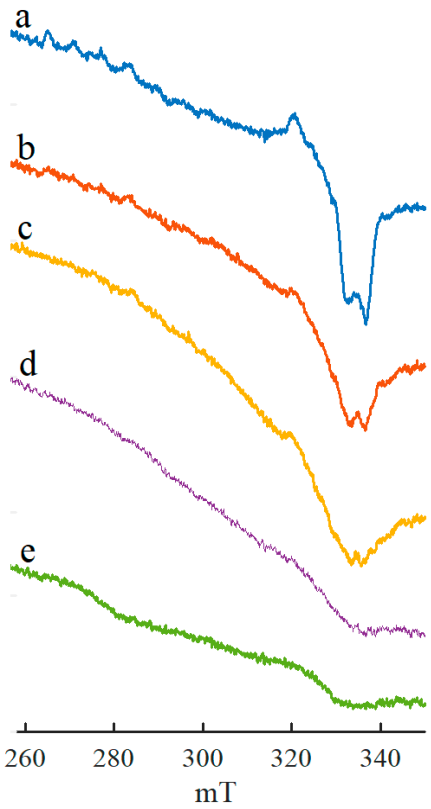

Figure 7. EPR spectra of the $Co(acac)_2$–$AlEt_3$ catalytic system formed in toluene in a argone atmosphere in the presence of: (a–d) 1-hexene, (e) styrene; (a,e) 0.1–0.5 min, (b) 1–3 min, (c) 3–5 min, (d) 5–7 min after mixing the components. Spectra were obtained under identical conditions.

Therefore, to obtain additional information about cobalt-containing centres in the hydrogenation of model substrates, we have performed the experiments combining kinetic analysis, TEM, and EPR [69,77]. The combination of EPR spectroscopy and kinetic studies has shown the absence of a cymbate relationship between the concentration of paramagnetic complexes recorded in the EPR spectra and the catalytic activity of the employed systems in the hydrogenation of styrene. On the other hand, the appearance and growth of hydrogenation catalytic activity are associated with a pronounced ferromagnetic resonance signal. At the same time, for these samples, cobalt-containing nanoparticles were detected using TEM. This may be due to the fact that, under the conditions of catalytic hydrogenation, paramagnetic cobalt-containing structures are transformed to a more stable state, the nanoscale state. Noteworthy, to impart catalytic activity to the systems based on $Co(acac)_2$–$AlEt_3$, the proton-donor compounds are required [69,77]. It is established that $AlEt_3$ molecules in these specifics act not only as reducing agents and stabilizers of the formed particles, but as a catalytic poison. Regardless of structural peculiarities of $AlEt_3$ surface compounds with cobalt, $AlEt_3$ exerts a poisoning effect on the hydrogenation activity. The addition of proton-donor compounds suppresses the inhibitory effect. Simultaneously with hydrogenation, aggregation of cobalt-containing particles occurs due to their low stability in hydrocarbon media, which gradually decreases the catalytic activity owing to the reduction of the amount of the most active coordinatively unsaturated centres.

If proton-donor compounds are not added to the systems formed on the basis of $Co(acac)_2$–$AlEt_3$, a signal of paramagnetic cobalt-containing structures (see above) is first observed, which is eventually transformed into a low-intensity and broadened ferromagnetic resonance signal. At the same time, contrast structures are absent in the TEM micrographs, and catalytic activity during the performance of kinetic experiments is lacking.

3. Discussion

All the above spectra (Figures 1–7) show experimentally obtained results. To confirm the reliability of the spectral interpretation, mathematical simulation is required. In this work, the "EasySpin" module of the Matlab package [86] was employed, which takes into account only the electronic Zeeman and hyperfine coupling in the first order of approximation.

Previously [69,77], the EPR spectra of the systems formed on the basis of $Co(acac)_2$–$AlEt_3$ were simulated. It was assumed [87,88] that the spectrum presented in Figure 1a is a biaxially anisotropic signal with the following g-factor parameters: $g_{\perp} = 2.050$, $g_{\parallel} = 2.355$ (Figure 8a and Supplementary Material). Comparison of the real and simulated spectra, as well as the treatment of all other spectra shown in Figures 1–7 call into question the accuracy of these assumptions.

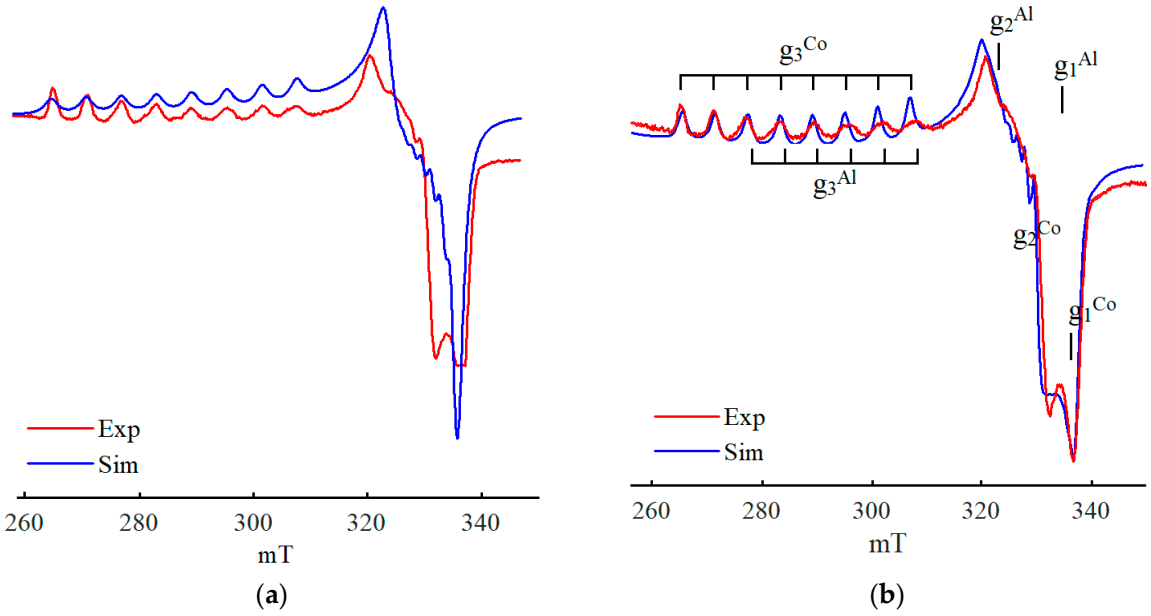

Figure 8. Real (red line) and simulated (blue line) EPR spectra of the $Co(acac)_2$–$AlEt_3$ catalytic system formed in toluene in an argon atmosphere (T = 77 K): (**a**) from [69,77], (**b**) made for this work.

The above spectra of the systems formed in the presence of Li-*n*-Bu or $(PhCH_2)MgCl$ (see Figure 4) differ from those of the system formed with $AlEt_3$ by the g_3 region. In the case of Li-*n*-Bu, three of the eight signals, and in the case of $(PhCH_2)MgCl$, four of the eight signals, are fused. This fact can be explained by the overlapping of two different EPR signals corresponding to two geometrically different paramagnetic structures.

In the simulation performed in this work, we considered the possible formation of not only paramagnetic cobalt-containing structures, since for the studied multicomponent systems, paramagnetic centres based on aluminium (^{27}Al, Nuclear spin 2.5, Natural abundance 100%), lithium (^{7}Li, Nuclear spin 1.5, Natural abundance 92.41%) and magnesium (^{25}Mg, Nuclear spin 2.5, Natural abundance 10%) can also be generated depending on the nature of the used cocatalyst [86]. Previously published articles [69,77] did not account for such a possibility. Meanwhile, the works [69,77] reported the EPR spectra recorded at room temperature for the $Co(acac)_2$–$AlEt_3$ systems (see Figure 9 and Supplementary Material), which were described as a combination of a low-intense ferromagnetic resonance signal from $[Co]_n$ and a signal with a hyperfine structure due to the interaction of an unpaired electron with the nuclei of cobalt, aluminium and hydrogen atoms.

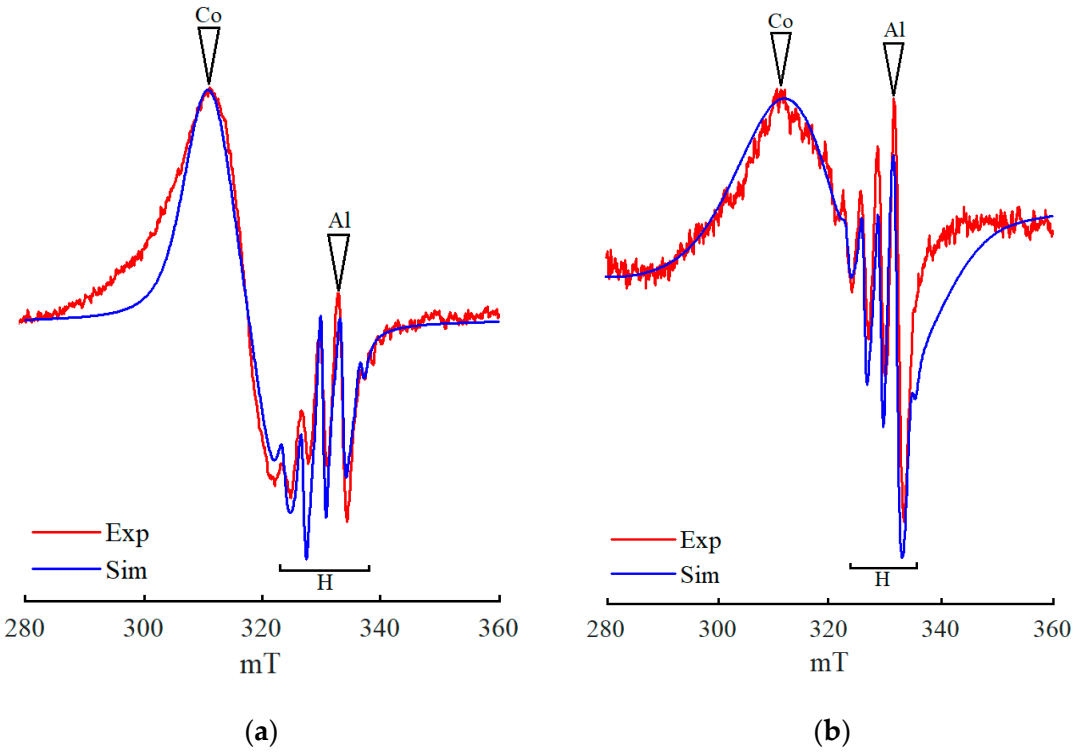

Figure 9. Real (red line) and simulated (blue line) EPR spectrum of the $Co(acac)_2$–$AlEt_3$ catalytic system formed in hexane in the presence of: (**a**) toluene, (**b**) durene, recorded at 293 K. Spectrum (**a**) was taken from [69,77].

In other words, such an EPR spectrum can be interpreted as the coordination of cobalt-containing nanoparticles with the $AlEt_2(acac)$ radical:

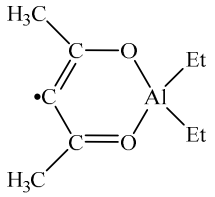

The stabilization of $AlEt_2(acac)$ in the Co(0) coordination sphere is additionally confirmed by the fact that the rate of the interaction between $AlEt_3$ and $AlEt_2(acac)$ in the presence of Co(0) structures is by 1.7 times lower than that of the interaction between $AlEt_3$ and $AlEt_2(acac)$ in the absence of cobalt, according to UV spectroscopy data [69].

Figure 8b depicts the real and simulated spectra of the $Co(acac)_2$–$AlEt_3$ system formed in toluene. The simulation was performed for a structure containing both paramagnetic cobalt and aluminium centres. In addition, a component corresponding to a low-intensity, broadened ferromagnetic resonance signal was included in the simulation model. The cobalt structure is presented by a triaxial anisotropic signal with the following g-factor parameters: g_1 = 2.0170, g_2 = 2.07131, g_3 = 2.354 (see Table S2). That is, Co(0) is in a tetragonal field with rhombic distortion.

When $AlEt_3$ was replaced by $AlEt_2(OEt)$ or when crystalline hydrates $Co(acac)_2 \cdot 0.5H_2O$ or $Co(acac)_2 \cdot 3.0H_2O$ were used instead of $Co(acac)_2$, the shape of the spectrum changed (see Figure 5). This is easy to explain, since the interaction of water molecules with organoaluminium compounds affords aluminoxane-like products [89], which are close to $AlEt_2(OEt)$ molecules. In turn, changes the geometry of the resulting paramagnetic structures and distorts the signal in the EPR spectrum. Figure 10 shows real and simulated spectra for

systems based on $AlEt_3$ and $Co(acac)_2 \cdot 0.5H_2O$ or $Co(acac)_2 \cdot 3.0H_2O$, respectively. The simulation was also carried out for the structures containing paramagnetic centres of cobalt and aluminium, in combination with a component corresponding to the ferromagnetic resonance signal.

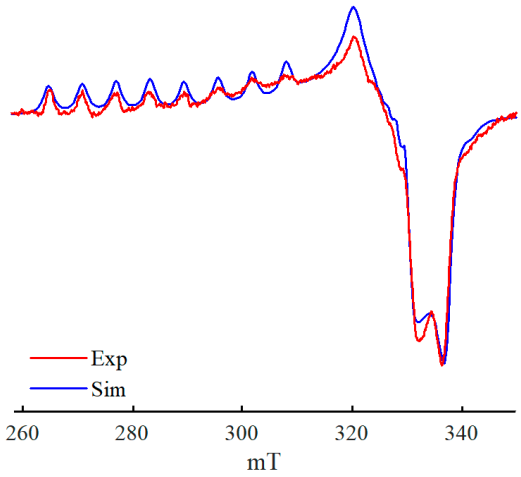

Figure 10. Real (red line) and simulated (blue line) EPR spectra of the catalytic system formed in toluene and in an argon atmosphere on the base of $AlEt_3$ and $Co(acac)_2 \cdot 3.0H_2O$, recorded at T = 77 K.

Similar simulations were implemented for the systems formed in the presence of Li-*n*-Bu or $(PhCH_2)MgCl$ (see Figure 11). In this case, the simulation model of paramagnetic centres also included lithium and magnesium atoms, respectively, and the ferromagnetic resonance signal. The simulated EPR spectra corresponding to each specific component (excluding the ferromagnetic resonance one) as well as the combination of components for each of the considered catalytic systems are given in the Supplementary Material (Figures S2–S4).

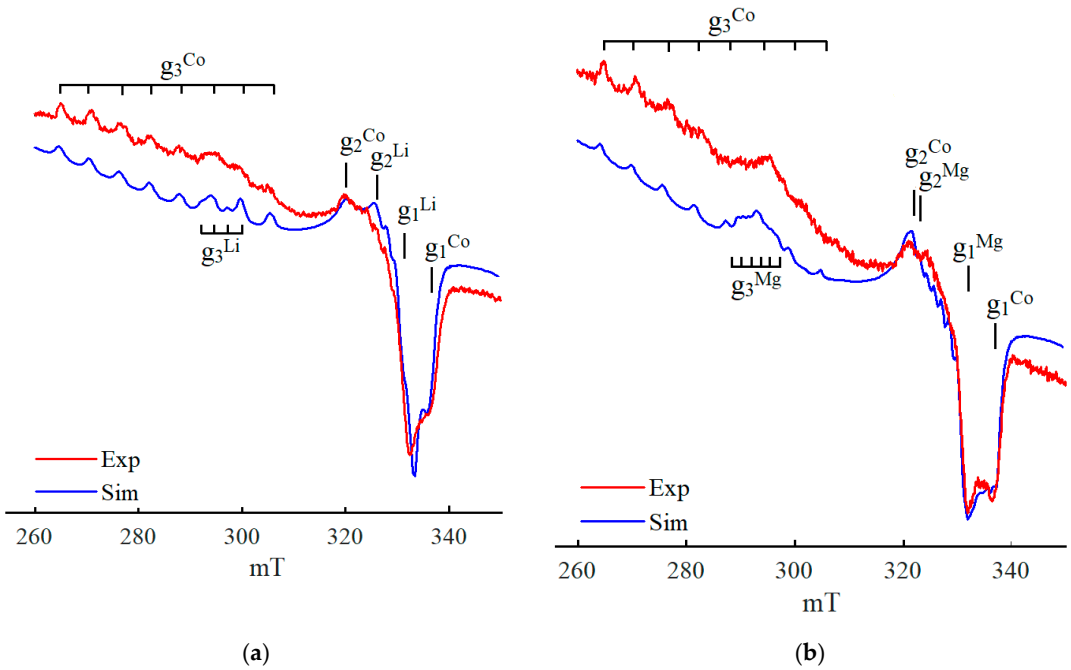

Figure 11. Real (red line) and simulated (blue line) EPR spectra of the catalytic system formed in toluene and in an argon atmosphere on the base of $Co(acac)_2$ and (**a**) Li-*n*-Bu or (**b**) $PhCH_2)MgCl$, recorded at T = 77 K.

It should be noted that a possible alternative to the above model assumes that the presented spectra contain at least two cobalt complexes with different g_3 parameters. Therefore, a series of experiments were carried out, in which the combination of several types of cocatalysts were attempted (the order of mixing the reagents, the time of interaction of each of the reagents with each other, the sampling duration, and the nature of the different solvents were varied). The experiments with mixing two systems, e.g., $Co(acac)_2$-$AlEt_3$ and $Co(acac)_2$-LiBu, formed separately, were carried out. Unfortunately, attempts to obtain reproducible results failed. Most likely, this is due to the high reactivity of the cocatalysts, which can not only react with the cobalt complex, but also affect each other. Therefore, the interpretation of the considered EPR spectra as a combination of signals from at least two cobalt complexes with different g_3 parameters remains a debatable question.

4. Models of Paramagnetic Site

The performed computations permit to conclude that the paramagnetic complexes, formed via the interaction of the initial components of the studied systems, should include both cobalt (in the zero-oxidation state, with electronic configuration $3d^9$) and paramagnetic centres of the corresponding non-transition metals. The entire array of data presented in the paper allows us to deduce an inference that if the arene is a six-electron ligand and the alkyl group is a one-electron ligand, then acetylacetonate should be considered as a two-electron ligand taking into account the 18-electron rule [90,91]. Next, it can be assumed that cobalt is coordinated to the double bond of the carbonyl group, and non-transition metal is coordinated to the carbonyl oxygen due to the donor–acceptor interaction between the lone electron pair of the oxygen atom and the vacant orbital of a non-transition metal, for example, aluminium. The coordination of an organometallic compound with a cobalt atom occurs due to the formation of a polycentric electron-deficient bond, which, apart from the atoms of transition and non-transition metals and the α-carbon atom of the alkyl group of the cocatalyst, also contains an oxygen atom. These data support the previously proposed model (see Figure 12).

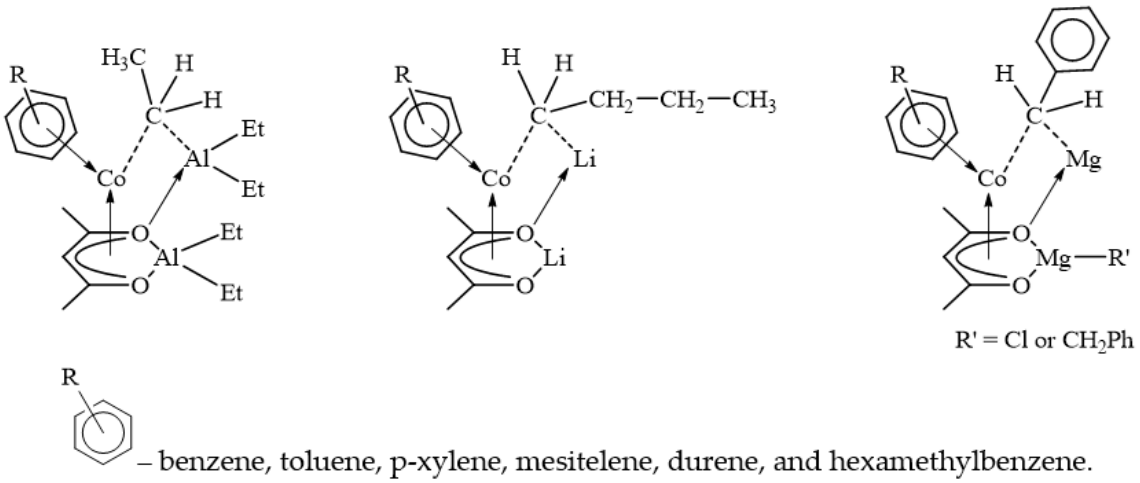

Figure 12. Models of bimetallic paramagnetic complexes formed during the interaction of components of systems based on $Co(acac)_2$ and Red (where Red = $AlEt_3$, Li-*n*-Bu, $(PhCH_2)MgCl$). The model with $AlEt_3$ taken from [69,77].

Given that the intermediates described in this paper are highly active compounds, which can be observed only by EPR spectroscopy at T = 77 K, the quantum-chemical calculations could give an additional insight into the studied structures. However, at this stage, there are no reliable algorithms for calculation of structures bearing an open electron shell. So far, there are only a few examples performed using density functional theory (DFT) that prove that such calculations are in principle possible [49,92,93]. Therefore, additional

data on such structures are planned to be obtained using the EPR technique at 4–280 K, as well as pulsed EPR procedures.

The formation of the intermediates can hardly be rationalized using the ^{59}Co or ^{27Al}/[^{7}Li and/or ^{6}Li]/^{25}Mg NMR spectroscopy. The ^{59}Co or ^{27}Al/[^{7}Li and/or ^{6}Li]/^{25}Mg atoms are quadrupole; therefore, the characteristic signal widths increase in an asymmetric environment, which makes such studies uninformative. Nevertheless, the literature analysis evidences that such paramagnetic structures in principle can be studied by the ^{59}Co NMR [94,95], ^{27}Al NMR [96,97], ^{7}Li and/or ^{6}Li [98,99], as well as ^{25}Mg NMR spectroscopy [100,101]. However, each specific compound has unique parameters of the corresponding NMR spectra, and a lot of experimental work is required to interpret these structures.

In addition, it should be emphasized that, firstly, the metal-arene bond weakens in the series of Fe > Co > Ni [84], and secondly, the electronic configuration of the outer electron shell of the nickel atom differs from that of the cobalt shell. Therefore, the realization of a structure similar to that shown in Figure 12 is likely impossible for nickel.

The formation of nano-sized catalytically active structures in hydrogenation catalysis can be represented as follows (see Scheme 1):

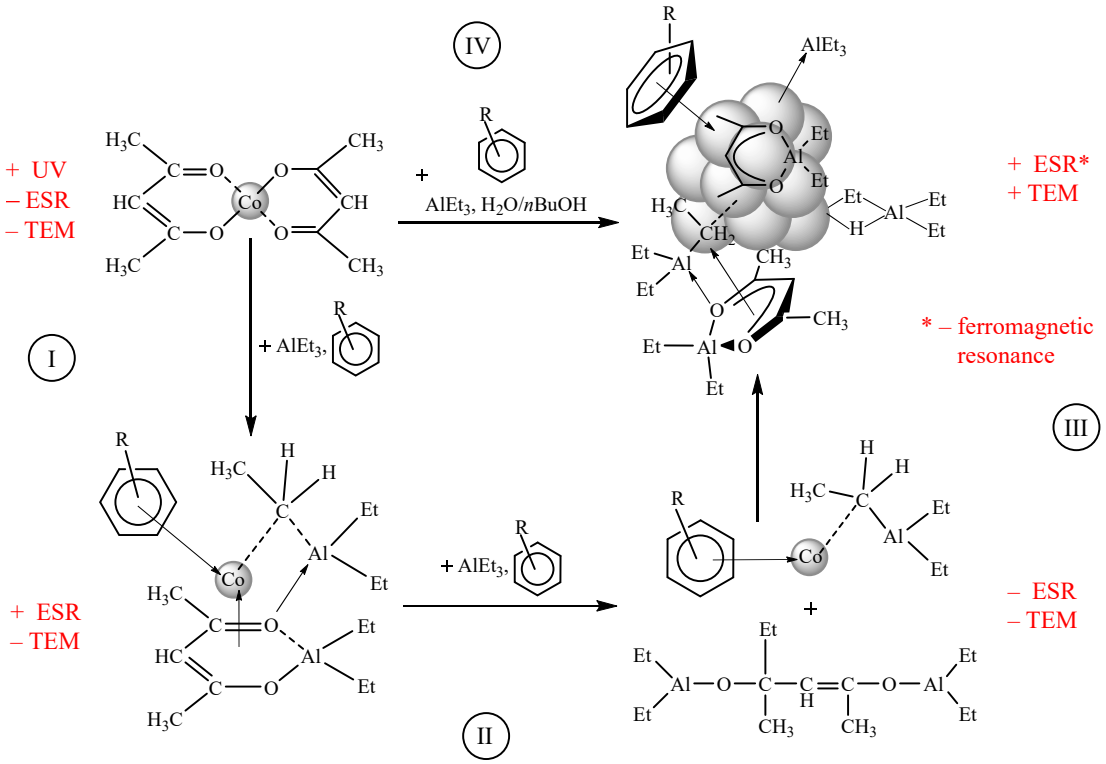

Scheme 1. Formation of nano-sized multi-component catalytically active structures in hydrogenation catalysis based on the $Co(acac)_2$–$AlEt_3$ system.

A solution of $Co(acac)_2$ in arenes or in saturated hydrocarbons with arenes has a characteristic signal in the UV spectrum: λ_{max} = 288 $_{HM}$, ε_{288} = 16 200 L (mol cm)$^{-1}$. Accordingly, transformation (I, Scheme 1) can be monitored in descending order or by complete disappearance of this signal. As shown above, the formation of bimetallic paramagnetic structures containing Co(0) is easily detected using the EPR spectroscopy. Meanwhile, the formation of LCo(Ar) (where Ar—arene, L = $AlEt_3$ and/or $AlEt_2(acac)$) (II, Scheme 1) structures and even their existence as a matter of fact is a theoretical conclusion. Since, in this case, cobalt is also formally Co(0), it should be visible by the EPR spectroscopy. However, new signals were not detected. Therefore, it can be assumed that the LCo(Ar) structures dimerize to form diamagnetic (via the interaction of two molecules of the Co(0)

complex), etc. compositions. When they reach a critical concentration, these compositions give nano-sized compounds (III, Scheme 1), which appear in the EPR spectrum by the ferromagnetic resonance signals, and on TEM micrographs, they are observed as high-contrast structures. At the moment, it seems impossible to make more reasonable assumption. The implementation of path IV (see Scheme 1) was previously described in detail [69,70,77].

5. Materials and Methods

Experimental methods for the preparation of the starting reagents and gases, synthetic protocols and procedures of the starting components interaction, as well as performing the kinetic, EPR and TEM HR experiments have been discussed in detail [69,77] and in the Supplementary Material.

6. Conclusions

In conclusion, the dynamics of the initial compound transformation into paramagnetic bimetallic intermediates acting as precursors of catalytically active sites has been studied for the first time using the example of multicomponent hydrogenation systems $Co(acac)_2$ and Red (where Red = $AlEt_3$, $AlEt_2(OEt)$, Li-*n*-Bu, $(PhCH_2)MgCl$). Despite the fact that the intermediates formed in multicomponent systems under the conditions of oligo- and/or polymerization of α-olefins have been thoroughly described, hydrogenation systems in this sense are poorly investigated. This is due to the high reactivity of such intermediates, and to the fact that the hydrogenation systems are very sensitive to air or moisture. Consequently, for the correct interpretation of the obtained experimental data, one should clearly understand the meaning of each specific experimental fact, as well as the significance of the results obtained for planning further research work. In this particular case, it is possible not only to detect intermediates immediately for several catalytic systems, but also to monitor the features of their behaviour in dynamics, under a certain range of conditions. In addition, a large body of statistical information has been obtained in the course of the EPR experiments. The processing of all these data enables the suggestion that the intermediates bear two paramagnetic fragments, one of which contains a cobalt atom in a formally zero oxidation state (with the electronic configuration $3d^9$), stabilized by an arene molecule(s) and an acetylacetonate ligand, and the second has an aluminium, lithium or magnesium atom (depending on the nature of the cocatalyst used). The simultaneous combination of kinetic experiments with the EPR and TEM studies, as well as statistical processing of all data permits to explain and link together both the previously described results [66,69,77] and the findings are presented for the first time in this work.

The procedure of EPR experiments with multicomponent systems of catalytic hydrogenation, with an explanation of each subsequent experimental step, is reported in detail for the first time. The total route of mathematical modelling of the obtained spectra is presented. The scheme of all proposed transformations, occurring during the formation of the multicomponent catalytic hydrogenation systems, is presented for the first time. These findings can constitute the basis for the development of a general methodology for dynamic EPR spectroscopy of multicomponent catalytic hydrogenation systems.

Supplementary Materials: The following supporting information can be downloaded at: https://www.mdpi.com/article/10.3390/catal13040653/s1, Figure S1: Real (solid line) and simulated (dashed line) EPR spectra of the $Co(acac)_2$–$AlEt_3$ catalytic system formed in toluene in an argon atmosphere (a) T = 293 K, and (b) T = 77; Figure S2: Simulated subspectra of Al-containing fragment (a) and Co-containing fragment of (c) simulated spectrum shown in Figure 10; Figure S3: Simulated subspectra of Li-containing fragment (a) and Co-containing fragment of (c) simulated spectrum shown in Figure 11a; Figure S4: Simulated subspectra of Mg-containing fragment (a) and Co-containing fragment of (c) simulated spectrum shown in Figure 11b; Table S1: The EPR parameters of catalytic systems based on $Co(acac)_2$–Red–toluene, according to the data of works; Table S2:The data used to simulation of the EPR spectra of systems based on $Co(acac)_2$–Red in toluene. References [17,69,77,86,101–112] are cited in the Supplementary Materials.

Funding: Research completed in the framework of the Program of Fundamental Research.

Data Availability Statement: Data are contained within the article.

Acknowledgments: This article is especially dedicated to my teacher and scientific adviser F.K. Schmidt (Ir-kutsk State University) without whose constant support my scientific work was not possible. The studies were carried out using the equipment of the Center for Collective Use of Analytical Equipment of the Irkutsk State University, accessed on 1 July 2020 (http://ckp-rf.ru/ckp/3264/). The author is grateful to the Baikal Analytical Center for Collective Uses, SB RAS. The author would like to express their sincere gratitude to the co-author of the publications from Irkutsk State University F.K. Shmidt.

Conflicts of Interest: The author declare no conflict of interest.

References

1. Bertrand, P. *Electron Paramagnetic Resonance Spectroscopy*; Springer Nature: Basel, Switzerland, 2020; pp. 1–420.
2. Perera, K.P.U.; Smith, D.W. In Situ EPR Spectroscopy of Aromatic Diyne Cyclopolymerization. *J. Org. Chem.* **2004**, *49*, 6124–6127. [CrossRef]
3. Liu, F.; Karoui, H.; Rockenbauer, A.; Liu, S.; Ouari, O.; Bardelang, D. EPR Spectroscopy: A Powerful Tool to Analyze Supramolecular Host—Guest Complexes of Stable Radicals with Cucurbiturils. *Molecules* **2020**, *25*, 776. [CrossRef]
4. Peyrot, F.; Lajnef, S.; Versace, D. Electron Paramagnetic Resonance Spin Trapping (EPR–ST) Technique in Photopolymerization Processes. *Catalysts* **2022**, *12*, 772. [CrossRef]
5. Pietrzyk, P.; Mazur, T.; Sojka, Z. Electron Paramagnetic Resonance Spectroscopy of Inorganic Materials. In *Local Structural Characterisation: Inorganic Materials Series*; Bruce, D.W., O'Hare, D., Walton, R., Eds.; John Wiley & Sons, Ltd.: Hoboken, NJ, USA, 2013; pp. 225–301.
6. Boere, T. Inorganic and Organometallic Radicals of Main Group Elements. In *Electron Paramagnetic Resonance*; RSC Publishing: London, UK, 2013; Volume 23, pp. 22–57. [CrossRef]
7. Bracci, M.; Van Doorslaer, S.; García, I. *EPR of Compound I: An Illustrated Revision of the Theoretical Model*; Springer: Vienna, Austria, 2020; Volume 51, pp. 1559–1589, ISBN 0123456789.
8. Prosser, K.E.; Walsby, C.J. Electron Paramagnetic Resonance as a Tool for Studying the Mechanisms of Paramagnetic Anticancer Metallodrugs. *Eur. J. Inorg. Chem.* **2017**, *2017*, 1573–1585. [CrossRef]
9. Cutsail, G.E. Applications of Electron Paramagnetic Resonance Spectroscopy to Heavy Main-Group Radicals. *Dalt. Trans.* **2020**, *49*, 12128–12135. [CrossRef]
10. Dasgupta, A.; Richards, E.; Melen, R.L. Frustrated Radical Pairs: Insights from EPR Spectroscopy. *Angew. Chem. Int. Ed.* **2021**, *133*, 53–65. [CrossRef]
11. Schmidt, M.J.; Fedoseev, A.; Summerer, D.; Drescher, M. Genetically Encoded Spin Labels for In Vitro and In-Cell EPR Studies of Native Proteins. In *Electron Paramagnetic Resonance Investigations of Biological Systems by Using Spin Labels, Spin Probes, and Intrinsic Metal Ions, Part A*, 1st ed.; Elsevier Inc.: Amsterdam, The Netherlands, 2015; Volume 563, pp. 483–502.
12. Klare, J.P. *Electron Paramagnetic Resonance of Membrane Proteins*, 3rd ed.; Elsevier Ltd.: Amsterdam, The Netherlands, 2017; pp. 442–446, ISBN 9780124095472.
13. Universit, A.M. Probing Conformational Changes and Interfacial Recognition Site of Lipases with Surfactants and Inhibitors. *Methods Enzymol.* **2017**, *583*, 279–307. [CrossRef]
14. Yordanov, N.D. Quantitative EPR Spectrometry—"State of the Art". *Appl. Magn. Reson.* **1994**, *6*, 241–257. [CrossRef]
15. Nagy, V. Quantitative EPR: Some of the Most Difficult Problems. *Appl. Magn. Reson.* **1994**, *6*, 259–285. [CrossRef]
16. Mazúr, M.; Valko, M.; Pelikán, P. Quantitative EPR Spectroscopy in Solid State Chemistry. *Chem. Pap.* **1997**, *51*, 134–136.
17. Eaton, G.R.; Eaton, S.S.; Barr, D.P.; Weber, R.T. *Quantitative EPR*; Springer: Vienna, Austria, 2010; p. 1985.
18. Fendorf, S.E.; Sparks, D.L.; Franz, J.A.; Camaioni, D.M. Electron Paramagnetic Resonance Stopped-Flow Kinetic Study of Manganese (II) Sorption—Desorption on Birnessite. *Soil Sci. Soc. Am. J.* **1985**, *57*, 57–62. [CrossRef]
19. Hu, Y.; Norton, J.R. Kinetics and Thermodynamics of H–/H•/H+ Transfer from a Rhodium(III) Hydride. *J. Am. Chem. Soc.* **2014**, *136*, 5938–5948. [CrossRef] [PubMed]
20. Schubert, E.; Hett, T.; Schiemann, O.; Nejatyjahromy, Y. EPR Studies on the Kinetics of the α-Hydroxyethyl Radical Generated by Fenton-like Chemistry. *J. Magn. Reson.* **2016**, *265*, 10–15. [CrossRef] [PubMed]
21. Jeschke, G. EPR Techniques for Studying Radical Enzymes. *Biochim. Biophys. Acta* **2005**, *1707*, 91–102. [CrossRef] [PubMed]
22. Goswami, M.; Chirila, A.; Rebreyend, C. EPR Spectroscopy as a Tool in Homogeneous Catalysis Research. *Top. Catal.* **2015**, *58*, 719–750. [CrossRef]
23. Rhodes, C.J. The Role of ESR Spectroscopy in Advancing Catalytic Science: Some Recent Developments. *Prog. React. Kinet. Mech.* **2015**, *40*, 201–248. [CrossRef]
24. Behrens, M.; Zander, S.; Kurr, P.; Jacobsen, N.; Senker, J.J.; Koch, G.; Ressler, T.; Fischer, R.W.; Schlögl, R.; Schlo, R.; et al. Performance Improvement of Nanocatalysts by Promoter-Induced Defects in the Support Material: Methanol Synthesis over Cu/ZnO:Al. *J. Am. Chem. Soc.* **2013**, *135*, 6061–6068. [CrossRef]

25. Selim, M.M.; Abd El-Maksoud, I.H.; El-maksoud, I.H.A. Spectroscopic and Catalytic Characterization of Ni Nano-Size Catalyst for Edible Oil Hydrogenation. *Microporous Mesoporous Mater.* **2005**, *85*, 273–278. [CrossRef]
26. Shim, H.; Dutta, P.; Seehra, M.S.; Bonevich, J. Size dependence of the blocking temperatures and electron magnetic resonance spectra in NiO nanoparticles. *Solid State Commun.* **2008**, *145*, 192–196. [CrossRef]
27. Lucarini, M.; Pasquato, L. ESR Spectroscopy as a Tool to Investigate the Properties of Self-Assembled Monolayers Protecting Gold Nanoparticles. *Nanoscale* **2010**, *2*, 668–676. [CrossRef]
28. Alonso, F.; Riente, P.; Sirvent, J.A.; Yus, M. Nickel Nanoparticles in Hydrogen-Transfer Reductions: Characterisation and Nature of the Catalyst. *Appl. Catal. A Gen.* **2010**, *378*, 42–51. [CrossRef]
29. Alley, W.M.; Hamdemir, I.K.; Johnson, K.A.; Finke, R.G. Ziegler-Type Hydrogenation Catalysts Made from Group 8–10 Transition Metal Precatalysts and AlR_3 Cocatalysts: A Critical Review of the Literature. *J. Mol. Catal. A Chem.* **2010**, *315*, 1–27. [CrossRef]
30. Claverie, J.P.; Schaper, F. Ziegler-Natta Catalysis: 50 Years after the Nobel Prize. *MRS Bull.* **2013**, *38*, 213–218. [CrossRef]
31. Nifant, I.; Ivchenko, P.; Tavtorkin, A.; Vinogradov, A. Non-Traditional Ziegler-Natta Catalysis in α -Olefin Transformations: Reaction Mechanisms and Product Design. *Pure Appl. Chem.* **2017**, *89*, 1017–1032. [CrossRef]
32. Klaue, A.; Kruck, M.; Friederichs, N.; Bertola, F.; Wu, H.; Morbidelli, M. Insight into the Synthesis Process of an Industrial Ziegler-Natta Catalyst. *Ind. Eng. Chem. Res.* **2019**, *58*, 886–896. [CrossRef]
33. Deng, L.; Woo, T.K.; Cavallo, L.; Margl, P.M.; Ziegler, T.; January, R.V.; Re, V.; Recei, M.; April, V. The Role of Bulky Substituents in Brookhart-Type Ni(II) Diimine Catalyzed Olefin Polymerization: A Combined Density Functional Theory and Molecular Mechanics Study. *J. Am. Chem. Soc.* **1997**, *119*, 6177–6186. [CrossRef]
34. Jeon, M.; Kim, S.Y. Ethylene Polymerizations with Unsymmetrical (α-Diimine)Nickel(II) Catalysts. *Polym. J.* **2008**, *40*, 409–413. [CrossRef]
35. Wang, F.; Chen, C. A Continuing Legend: The Brookhart-Type α-Diimine Nickel and Palladium Catalysts. *Polym. Chem.* **2019**, *10*, 2354–2369. [CrossRef]
36. Bruckner, A. In Situ Electron Paramagnetic Resonance: A Unique Tool for Analyzing Structure–Reactivity Relationships in Heterogeneous Catalysis. *Chem. Soc. Rev.* **2010**, *39*, 4673–4684. [CrossRef]
37. Rabeah, J.; Radnik, J.; Briois, V.; Maschmeyer, D.; Stochniol, G.; Peitz, S.; Reeker, H.; La Fontaine, C.; Brückner, A.; Rabeah, J.; et al. Tracing Active Sites in Supported Ni Catalysts during Butene Oli-Gomerization by Operando Spectroscopy under Pressure Tracing Active Sites in Supported Ni Catalysts during Butene Oligomerization by Operando Spectroscopy under Pressure. *ACS Catal.* **2016**, *6*, 8224–8228. [CrossRef]
38. Liu, Y.; Wang, R. In Situ Electron Paramagnetic Resonance Spectroscopy in Catalysis. In *Heterogeneous Catalysts: Advanced Design, Characterization and Applications*; Teoh, W.Y., Urakawa, A., Ng, Y.H., Sit, P., Eds.; Wiley-VCH: Weinheim, Germany, 2021; pp. 295–310.
39. Zichittella, G.; Polyhach, Y.; Tschaggelar, R.; Jeschke, G.; Pérez-Ramírez, J. Quantification of Redox Sites during Catalytic Propane Oxychlorination by Operando EPR Spectroscopy. *Angew. Chem. Int. Ed.* **2021**, *60*, 3596–3602. [CrossRef] [PubMed]
40. Bryliakov, K.P.; Talsi, E.P. Frontiers of Mechanistic Studies of Coordination Polymerization and Oligomerization of α-Olefins. *Coord. Chem. Rev.* **2012**, *256*, 2994–3007. [CrossRef]
41. Dong, Q.; Yang, X.-J.; Gong, S.; Luo, Q.; Li, Q.-S.; Su, J.-H.; Zhao, Y.; Wu, B. Distinct Stepwise Reduction of a Nickel-Nickel-Bonded Compound Containing an α-Diimine Ligand: From Perpendicular to Coaxial Structures. *Chem. A Eur. J.* **2013**, *19*, 15240–15247. [CrossRef]
42. Takeuchi, D.; Osakada, K. Oligomerization of Olefins. In *Organometallic Reactions and Polymerization*; Osakada, K., Ed.; Springer: Berlin/Heidelberg, Germany, 2014; pp. 169–215.
43. Shmidt, F.K.; Titova, Y.Y.; Belykh, L.B. The Role of Phosphine and 1,2-Diimine Complexes of Nickel in the Oxidation States 0, +1, and +2 in the Catalyzed Di-, Oligo-, and Polymerization of Ethylene. *Kinet. Catal.* **2016**, *57*, 61–71. [CrossRef]
44. Olivier-Bourbigou, H.; Breuil, P.A.R.; Magna, L.; Michel, T.; Espada Pastor, M.F.; Delcroix, D. Nickel Catalyzed Olefin Oligomerization and Dimerization. *Chem. Rev.* **2020**, *120*, 7919–7983. [CrossRef]
45. Lee, H.; Bçrgel, J.; Ritter, T. Carbon—Fluorine Reductive Elimination from Nickel (III) Complexes. *Angew. Chem. Int. Ed.* **2017**, *56*, 6966–6969. [CrossRef]
46. Matsubara, K.; Fukahori, Y.; Inatomi, T.; Tazaki, S.; Yamada, Y.; Koga, Y.; Kanegawa, S.; Nakamura, T. Monomeric Three-Coordinate N-Heterocyclic Carbene Nickel(I) Complexes: Synthesis, Structures, and Catalytic Applications in Cross-Coupling Reactions. *Organometallics* **2016**, *35*, 3281–3287. [CrossRef]
47. Mondal, P.; Pirovano, P.; Das, A.; Farquhar, E.R.; McDonald, A.R. Hydrogen Atom Transfer by a High-Valent Nickel-Chloride Complex. *J. Am. Chem. Soc.* **2018**, *140*, 1834–1841. [CrossRef]
48. Gao, W.; Xin, L.; Hao, Z.; Li, G.; Su, J.-H.; Zhou, L.; Mua, Y.; Mu, Y. The Ligand Redox Behavior and Role in 1,2-Bis[(2,6-Diisopropylphenyl)Imino]-Acenaphthene Nickel–TMA(MAO) Systems for Ethylene Polymerization. *Chem. Commun.* **2015**, *51*, 7004–7007. [CrossRef]
49. Schwab, M.M.; Himmel, D.; Kacprzak, S.; Radtke, V.; Kratzert, D.; Weis, P.; Wernet, M.; Peter, A.; Yassine, Z.; Schmitz, D.; et al. Synthesis, Characterisation and Reactions of Truly Cationic Ni(I) -Phosphine Complexes. *Chem. A Eur. J.* **2018**, *98*, 1823–1833. [CrossRef]
50. Do, L.H.; Labinger, J.A.; Bercaw, J.E. Spectral Studies of a Cr(PNP)–MAO System for Selective Ethylene Trimerization Catalysis: Searching for the Active Species. *ACS Catal.* **2013**, *3*, 2582–2585. [CrossRef]

51. Friedfeld, M.R.; Margulieux, G.W.; Schaefer, B.A.; Chirik, P.J. Bis(Phosphine)Cobalt Dialkyl Complexes for Directed Catalytic Alkene Hydrogenation. *J. Am. Chem. Soc.* **2014**, *136*, 13178–13181. [CrossRef]
52. Lin, T.-P.; Peters, J.C. Boryl–Metal Bonds Facilitate Cobalt/Nickel-Catalyzed Olefin Hydrogenation. *J. Am. Chem. Soc.* **2014**, *136*, 13672–13683. [CrossRef]
53. Noveron, C.; Herradora, R.; Olmstead, M.M.; Mascharak, P.K. Low-Spin Iron(III) Complexes with N,S Coordination: Syntheses, Structures, and Properties of Bis(N-2-Mercaptophenyl-2′-Pyridylmethyleniminato)Iron(III) Tetraphenylborate and Bis(N-2-Mercapto-2-Methylpropyl-2′-Pyridylmethyleniminato)Iron(III) Tetraphenylbo. *Inorg. Chim. Acta* **1999**, *285*, 269–276. [CrossRef]
54. Zadrozny, J.M.; Greer, S.M.; Freedman, D.E. Chemical Science Splitting Is Resistant to Structural Variation. *Chem. Sci.* **2016**, *7*, 416–423. [CrossRef] [PubMed]
55. Sakaki, S.; Yanase, Y.; Hagiwara, N.; Takeshita, T.; Naganuma, H.; Ohyoshi, A.; Ohkubo, K. ESR and MO Studies of Some C4v Symmetrical Ruthenium(III) Complexes. *J. Phys. Chem.* **1982**, *86*, 1038–1043. [CrossRef]
56. Frantz, S.; Weber, M.; Scheiring, T.; Fiedler, J.; Duboc, C.; Kaim, W. Mechanism and Product Characterization from the Electroreduction of Heterodinuclear Complexes $[(C_5Me_5)ClM(m\text{-}L)Re(CO)_3X](PF_6)$, M=Rh or Ir, L=2,2-Azobispyridine or 2,2-Azobis(5-Chloropyrimidine), X=halide. *Inorg. Chim. Acta* **2004**, *357*, 2905–2914. [CrossRef]
57. Knijnenburg, Q.; Horton, A.D.; van der Heijden, H.; Kooistra, T.M.; Hetterscheid, D.G.H.; Smits, J.M.M.; De Bruin, B.; Budzelaar, P.H.M.; Gal, A.W. Olefin Hydrogenation Using Diimine Pyridine Complexes of Co and Rh. *J. Mol. Catal. A Chem.* **2005**, *232*, 151–159. [CrossRef]
58. Fedushkin, I.L.; Skatova, A.A.; Ketkov, S.Y.; Eremenko, O.V.; Piskunov, A.V.; Fukin, G.K. [(Dpp-Bian)Zn-Zn(Dpp-Bian)]: A Zinc–Zinc-Bonded Compound Supported by Radical-Anionic Ligands. *Angew. Chemie Int. Ed.* **2007**, *46*, 4302–4305. [CrossRef] [PubMed]
59. Yu, R.P.; Darmon, J.M.; Milsmann, C.; Margulieux, G.W.; Stieber, S.C.E.; DeBeer, S.; Chirik, P.J. Catalytic Hydrogenation Activity and Electronic Structure Determination of Bis(Arylimidazol-2-Ylidene)Pyridine Cobalt Alkyl and Hydride Complexes. *J. Am. Chem. Soc.* **2013**, *135*, 13168–13184. [CrossRef] [PubMed]
60. Kokorin, A.I.; Landgraf, S.; Shapiro, A.B.; Grampp, G. EPR Spectroscopy of Mercury-Organic Compounds with Nitroxide Radicals. *Appl. Magn. Reason.* **2014**, *45*, 125–133. [CrossRef]
61. Carter, E.; Sharples, K.M.; Platts, J.A.; Murphy, D.M. Structure Determination of Bound Nitrogen-Based Adducts with Copper(II) Acetylacetonato; an EPR, ENDOR and DFT Study. *Phys. Chem. Chem. Phys.* **2015**, *17*, 11445–11454. [CrossRef] [PubMed]
62. Paul, R.; Buisson, P.; Joseph, N. Application Des Hydroborures Alcalins a La Preparation de Catalyseurs D'hydrogenation. *Comptes Rendus Hebd. Seances Acad. Sci.* **1951**, *232*, 627–629.
63. Polkovnikov, B.D.; Freidlin, L.K.; Balandin, A.A. Selective hydrogenation of adiponitrile over a cobalt boride catalyst. *Bull. Acad. Sci. USSR Div. Chem. Sci.* **1959**, *8*, 1436–1488. [CrossRef]
64. Brown, H.C.; Brown, C.A. A Simple Preparation of Highly Active Platinum Metal Catalysts for Catalytic Hydrogenation. *J. Am. Chem. Soc.* **1962**, *84*, 1494–1495. [CrossRef]
65. Alley, W.M.; Hamdemir, I.K.; Wang, Q.; Frenkel, A.I.; Li, L.; Yang, J.C.; Menard, L.D.; Nuzzo, R.G.; Ozkar, S.; Yih, K.-H.; et al. Industrial Ziegler-Type Hydrogenation Catalysts Made from $Co(Neodecanoate)_2$ or $Ni(2\text{-}Ethylhexanoate)_2$ and $AlEt_3$: Evidence for Nanoclusters and Sub-Nanocluster or Larger Ziegler-Nanocluster Based Catalysis. *Langmuir* **2011**, *27*, 6279–6294. [CrossRef]
66. Shmidt, F.K.; Nindakova, L.O.; Shainyanb, B.A.; Saraev, V.V.; Chipaninab, N.N.; Umanetz, V.A. Hydrogenation Catalysts Formation in the System $AlEt_3$-$Co(Acac)_{2,3}$. *J. Mol. Catal. A Chem.* **2005**, *235*, 161–172. [CrossRef]
67. Crooks, A.B.; Yih, K.-H.; Li, L.; Yang, J.C.; Özkar, S.; Finke, R.G. Unintuitive Inverse Dependence of the Apparent Turnover Frequency on Precatalyst Concentration: A Quantitative Explanation in the Case of Ziegler-Type Nanoparticle Catalysts Made from $[(1,5\text{-}COD)Ir(\mu\text{-}O_2C_8H_{15})]_2$. *ACS Catal.* **2015**, *5*, 3342–3353. [CrossRef]
68. Titova, Y.Y.; Belykh, L.B.; Shmidt, F.K. Ziegler-Type Nickel-Based Hydrogenation Catalysts: The Effect of the Water Content of the Nickel Precursor on the Size and Nature of the Resulting Particles. *Kinet. Catal.* **2016**, *57*, 388–393. [CrossRef]
69. Titova, Y.Y. Physico-Chemical Aspects of the Formation and Nature of the Activity of Systems Based on Cobalt, Nickel or Palladium Complexes in Hydrogenation and Oligomerization Reactions. Ph.D. Thesis, Irkutsk State University, Irkutsk, Russia, 2018. Available online: http://old.isu.ru/filearchive/dissert/ar_Titova.pdf (accessed on 1 February 2018).
70. Titova, Y.Y.; Schmidt, F.K. Directed Design of Hydrogenation Ziegler Systems. *New J. Chem.* **2021**, *45*, 4525–4533. [CrossRef]
71. Schmidt, F.K. *Hydrogenation and Dimerization Catalyzed by Complexes of First Row Transition Metals*; Gos. University: Irkutsk, Russia, 1986; p. 231.
72. Muetterties, E.L.L.; Rakowski, M.C.C.; Hirsekorn, F.J.J.; Larson, W.D.D.; Basus, V.J.J.; Anet, F.A.L.A.L. Hydrogenation of Arenes with Discrete Coordination Catalysts. III. I Synthesis and Nuclear Magnetic Resonance Spectrum of All-Cis-Cyclohexane-D6. *J. Am. Chem. Soc.* **1975**, *97*, 1266–1267. [CrossRef]
73. Stuhl, L.S.; DuBois; Rakowski, M.; Hirsekorn, F.J.; Bleeke, J.R.; Stevens, A.E.; Muetterties, E.L.; DuBois, M.R.; Hirsekorn, F.J.; Bleeke, J.R.; et al. Catalytic Homogeneous Hydrogenation of Arenes. 6. Reaction Scope for the (Tetta.3-2-Propenyl)Tris(Trimethyl Phosphite-P)Cobalt Catalyst. *J. Am. Chem. Soc.* **1978**, *100*, 2405–2410. [CrossRef]
74. Bleeke, J.R.; Muetterties, E.L. Catalytic Hydrogenation of Aromatic Hydrocarbons. Stereochemical Definition of the Catalytic Cycle for H_3-$C_3H_5Co(P(OCH_3)_3)_3$. *J. Am. Chem. Soc.* **1981**, *103*, 556–564. [CrossRef]
75. Jupp, A.R.; Stephan, D.W. New Directions for Frustrated Lewis Pair Chemistry. *Trends Cogn. Sci.* **2019**, *1*, 35–48. [CrossRef]
76. Paradies, J. From Structure to Novel Reactivity in Frustrated Lewis Pairs. *Coord. Chem. Rev.* **2019**, *380*, 170–183. [CrossRef]

77. Titova, Y.Y.; Belykh, L.B.; Shmidt, F.K. Preparation Method Effect on the Properties of Ziegler-Type Hydrogenation Catalysts Based on Bis(Acetylacetonato)Cobalt. *Kinet. Catal.* **2016**, *57*, 344–353. [CrossRef]
78. Titova, Y.Y.; Schmidt, F.K. Multicomponent Catalytic Systems for Di- and Oligomerization of Ethylene: New Mechanistic Aspects. *Catalysts* **2021**, *11*, 1489. [CrossRef]
79. Bauschlicher, C.W.; Partridge, H.; Langhoff, S.R. Theoretical Study of Transition-Metal Ions Bound to Benzene. *J. Phys. Chem.* **1992**, *96*, 3273–3278. [CrossRef]
80. Pandey, R.; Rao, B.K.; Jena, P.; Blanco, M.A. Electronic Structure and Properties of Transition Metal—Benzene Complexes. *J. Am. Chem. Soc.* **2001**, *123*, 3799–3808. [CrossRef]
81. Chaquin, P.; Costa, D.; Lepetit, C.; Che, M. Structure and Bonding in a Series of Neutral and Cationic Transition Metal−Benzene η^6 Complexes $[M(\eta^6\text{-}C_6H_6)]^{N+}$ (M = Ti, V, Cr, Fe, Co, Ni, and Cu). Correlation of Charge Transfer with the Bathochromic Shift of the E_1 Ring Vibration. *J. Phys. Chem. A* **2001**, *105*, 4541–4545. [CrossRef]
82. Taylor, P.; Dargel, T.K.; Hertwig, R.H.; Koch, W. How Do Coinage Metal Ions Bind to Benzene? *Mol. Phys.* **1999**, *96*, 583–591. [CrossRef]
83. Pampaloni, G. Aromatic Hydrocarbons as Ligands. Recent Advances in the Synthesis, the Reactivity and the Applications of Bis(η^6-Arene) Complexes. *Coord. Chem. Rev.* **2010**, *254*, 402–419. [CrossRef]
84. Shvydkiy, N.V.; Perekalin, D.S. Reactions of Arene Replacement in Transition Metal Complexes. *Coord. Chem. Rev.* **2020**, *411*, 213238. [CrossRef]
85. Pörschke, K.-R.; Kleimann, W.; Tsay, Y.-H.; Krüger, C.; Wilke, G. Zur Lewis-Acidität von Nickel(0). XII. Dimethylaluminiumhydrid-Komplexe von Nickel(0). *Chem. Ber.* **1990**, *123*, 1267–1273. [CrossRef]
86. Stoll, S.; Schweiger, A. EasySpin, a Comprehensive Software Package for Spectral Simulation and Analysis in EPR. *J. Magn. Reson.* **2006**, *178*, 42–55. [CrossRef] [PubMed]
87. Steinbock, O.; Neumann, B.; Cage, B.; Saltiel, J.; Mu, S.C.; Dalal, N.S. A Demonstration of Principal Component Analysis for EPR Spectroscopy: Identifying Pure Component Spectra from Complex Spectra. *Anal. Chem.* **1997**, *69*, 3708–3713. [CrossRef]
88. Rieger, P. *Electron Spin Resonance—Analysis and Interpretation*, 1st ed.; Royal Society of Chemistry: London, UK, 2007; p. 173.
89. Li, D.; Ma, F.; Guo, L.; Huang, J.; Zhang, Y.; Li, F.; Li, C. Polynuclear (α-Diimine) Nickel(II) Complex as Catalyst for Ethylene Oligomerization. *Appl. Organomet. Chem.* **2022**, *36*, e6509. [CrossRef]
90. Frenking, G.; Fro, N. The Nature of the Bonding in Transition-Metal Compounds. *Chem. Rev.* **2000**, *100*, 717–774. [CrossRef]
91. Zhao, L.; Pan, S.; Holzmann, N.; Schwerdtfeger, P.; Frenking, G. Chemical Bonding and Bonding Models of Main-Group Compounds. *Chem. Rev.* **2019**, *119*, 8781–8845. [CrossRef]
92. Schwab, M.M.; Himmel, D.; Kacprzak, S.; Radtke, V.; Weis, P.; Ray, K.; Scheidt, E.W.; Scherer, W.; de Bruin, B.; Krossing, W.S. $[Ni(cod)_2][Al(OR(F))_4]$, a Source for Naked Nickel(I) Chemistry. *Chem. A Eur. J.* **2015**, *54*, 14706–14709. [CrossRef]
93. Krylov, A.I. The Quantum Chemistry of Open-Shell Species. In *Reviews in Computational Chemistry*; Parrill, A.L., Lipkowitz, K.B., Eds.; John Wiley & Sons, Inc.: Hoboken, NJ, USA, 2017; Volume 30, pp. 151–224.
94. Yamasaki, A. Cobalt-59 Nuclear Magnetic Resonance Spectroscopy in Coordination Chemistry. *J. Coord. Chem.* **1991**, *24*, 211–260. [CrossRef]
95. Chan, J.C.C.; Au-Yeung, S.C.F. Cobalt-59 NMR Spectroscopy. *Annu. Rep. NMR Spectrosc.* **2000**, *41*, 1–54. [CrossRef]
96. Martineau, C.; Taulelle, F.; Group, T.; Lavoisier, I.; Umr, D.V.; De, U. The Use of ^{27}Al NMR to Study Aluminum Compounds: A Survey of the Last 25 Years. In *PATAI'S Chemistry of Functional Groups*; John Wiley & Sons, Ltd.: Hoboken, NJ, USA, 2016; pp. 1–51. [CrossRef]
97. Haouas, M.; Taulelle, F.; Martineau, C. Recent Advances in Application of Science Al NMR Spectroscopy to Materials. *Prog. Nucl. Magn. Reson. Spectrosc.* **2016**, *94–95*, 11–36. [CrossRef]
98. Bond, S.P.; Gelder, A.; Homer, J.; Mcwhinnie, W.R.; Perry, M.C. ^{6}Li Magic Angle Spinning Nuclear Magnetic Resonance Spectroscopy: A Powerful Probe for the Study of Lithium-Containing Materials. *J. Mater. Chem.* **1991**, *1*, 327–330. [CrossRef]
99. Davies, R.P. The Structures of Lithium and Magnesium Organocuprates and Related Species. *Coord. Chem. Rev.* **2011**, *255*, 1226–1251. [CrossRef]
100. Berm, B.R.; Lehmkuhl, H.; Mehler, K.; Rujinska, A. ^{25}Mg-NMR: A Method for the Characterization of Organomagnesium Compounds, Their Complexes, and Schlenk Equilibria. *Angen. Chrm. lnt. Ed.* **1984**, *23*, 534–535. [CrossRef]
101. Freitas, J.C.C.; Smith, M.E. Recent Advances in Solid-State ^{25}Mg NMR Spectroscopy. *Annu. Rep. NMR Spectrosc.* **2012**, *75*, 25–114. [CrossRef]
102. Gordon, A.J.; Ford, R.A. *Handbook of Practical Data, Techniques, and References*; Wiley: New York, NY, USA, 1972.
103. Mitchell, J.; Smith, D. *Aquametry: A Treatise on Methods for the Determination of Water*, 2nd ed.; Wiley: New York, NY, USA, 1977.
104. Perrin, D.D.; Armarego, W.L.F. *Purification of Laboratory Chemicals*; Pergamon: Oxford, UK, 1988.
105. *Preparativnaya Organicheskaya Khimiya (Preparative Organic Chemistry)*; Vul'fson, N.S. (Ed.) Khimiya: Moscow, Russia, 1964.
106. Ioffe, S.T.; Nesmeyanov, A.N. Metody Elementoorganicheskoi Khimii: Magnii, Berillii, Kal'tsii, Strontsii, Barii. In *Methods of Organoelement Chemistry: Magnesium, Beryllium, Calcium, Strontium, and Barium*; Akad. Nauk SSSR: Moscow, Russia, 1963.
107. Gilman, H.; Haubein, A.H. The Quantitative Analysis of Alkyllithium Compounds1. *J. Am. Chem. Soc.* **1944**, *66*, 1515–1516. [CrossRef]
108. Schuldt, B.; Heller, B.; Storz, F.; Madeja, K. Ziegler systems as hydrogenation catalysts. Part 1. $CoBr_2$/Li[AlH(O-/-butyl)$_3$]$_3$ system as a catalyst for the hydrogenation of anthracene. *J. Mol. Cat.* **1993**, *81*, 195–206. [CrossRef]

109. Ellern, J.B.; Ragsdale, R. Hexacoordinate Complexes of Bis (2, 4-Pentanedionato) Cobalt (II):[Bis (Acetylacetonato) Cobalt (II)]. *Inorg. Synth.* **1968**, *11*, 82–89.
110. Davis, C.M.; Curran, K.A. Manipulation of a Schlenk line: Preparation of tetrahydrofuran complexes of transition-metal chlorides. *J. Chem. Educ.* **2007**, *84*, 1822. [CrossRef]
111. McGarvey, B.R. Spin hamiltonian for Cr III complexes. Calculation from crystal field and molecular orbital models and ESR determination for some ethylenediammine complexes. *J. Chem. Phys.* **1964**, *41*, 3743–3758. [CrossRef]
112. Titova, Y.Y.; Shmidt, F.K. Role of Water in the Catalysis of Ethylene Di-and Oligomerization and Toluene Alkylation Reactions Based on Nickel Bis (Acetylacetonate) Systems. *Kinet. Catal.* **2017**, *58*, 749–757. [CrossRef]